The intrusive complex of the Island of Giglio: geomagnetic characteristics of plutonic facies with low susceptibility contrast

Osvaldo Faggioni([1])([2]), **David Westerman**([3]), **Fabrizio Innocenti**([1])([2]), **Nicolò Beverini**([1])([4]), **Cosmo Carmisciano**([1]), **Renzo Cavallini**([1]) **and Andrea Dini**([2])

([1]) *Istituto di Geofisica Marina, Consorzio Universitario della Spezia, Università di Pisa, La Spezia, Italy*

([2]) *Dipartimento di Scienze della Terra, Università di Pisa, Italy*

([3]) *Department of Geology, Norwich University, Northfield, VT, U.S.A.*

([4]) *Dipartimento di Fisica and INFM, Università di Pisa, Italy*

Abstract

Two main plutonic facies characterize the intrusive complex of the Island of Giglio, and the trend of their contact at depth has been modelled using a 2D½ analysis based on a detailed geomagnetic survey in order to verify the geological hypothesis of the subsurface geometry of this contact. The magnetic anomaly connected with the discontinuity is quite low, due to the small difference between the magnetic susceptibilities of the two granitic facies. Development of this model of inversion of the magnetic field, which is in good agreement with the geological interpretation, was made possible by: 1) accurate control of the geomagnetic time variations and consequent temporal reduction, 2) a very low level of the artificial magnetic noise, 3) high density of the magnetic survey, 4) detailed knowledge of the mapped geologic contact between facies and of their petrologic characteristics, and 5) direct local measurements of the magnetic susceptibilities of the key lithologies. The model shows the trends of the geological contact, as projected in three E-W sections, that dips eastward in the range between 21° and 54°, supporting the geologic hypothesis that the Pietrabona facies represents an external shell of the shallowly emplaced Giglio monzogranite intrusion.

Key words *plutonic facies – low susceptibility contrast – geomagnetic model*

1. Introduction

The Northern Tyrrhenian Sea and Western Tuscany represent an ensialic back-arc basin which developed within the inner (landward) portion of the Apennine chain as a result of extensive extensional tectonism of the Neogene age (Serri *et al.*, 1993). This area has been affected by igneous activity having complex genesis and evolution, forming a magmatic association known in the literature as the Tuscan Magmatic Province (TMP) (Marinelli, 1961; Innocenti *et al.*, 1992). The TMP includes a set of discordant acid plutons emplaced during the Upper Miocene and Pliocene at relatively high crustal levels (*e.g.*, Elba, Montecristo, Giglio, Gavorrano, etc.; Poli, 1992). These intrusive bodies have long been considered internally homogeneous, but recent geological investigations have revealed com-

Mailing address: Dr. Osvaldo Faggioni, Istituto di Geofisica Marina, Consorzio Universitario della Spezia, Università di Pisa, Via Fontevivo 25, Area IP, 19125 La Spezia, Italy; e-mail: cunispe@castagna.it

plex internal structures reflecting intricate emplacement histories (Bouillin *et al.*, 1993; Westerman *et al.*, 1993; Innocenti *et al.*, 1997).

The Giglio pluton is one of the TMP intrusions studied in greatest detail in recent times (Burelli and Papini, 1991; Passerini and Marcucci, 1992; Rossetti *et al.*, 1998); it is a monzogranite body in which, in spite of its relatively small size (about 20 km^2), two main mappable facies have been identified, and into which a small leucocratic body was subsequently emplaced (Westerman *et al.*, 1993).

This paper presents a geomagnetic survey which was carried out on the Giglio pluton in order to elucidate its internal structure, integrating the geomagnetic properties of the igneous mass with its geological and petrological features. The collected data revealed that it is possible to achieve high resolution in modelling the internal structure of the intrusion, in spite of a low susceptibility contrast between the different portions of the pluton.

2. Geological outlines

The Island of Giglio, located at 20 km from the Tuscan coast, is ellipsoidal with the major axis about 9 km long trending N20W; the minor axis is about 3 km in length. The island is surrounded by NNE-trending extensional basins that are partially filled by Neogene-Quaternary sedimentary deposits (Bartole, 1995). More than 90% of the island is underlain by intrusive rocks dominated by the Giglio monzogranite intrusion (GMI), into which a variety of widely distributed felsic dikes were intruded. The cooling age of the main intrusion, evaluated by Rb-Sr systematics, is 5 Ma. A small leucocratic pluton, the Scole monzogranite intrusion, also intruded the GMI along the mid-point of the eastern shoreline of the island (Westerman *et al.*, 1993).

A promontory on the western side of the island is underlain by three assemblages of Mesozoic rocks which have been described in detail by Lazzarotto *et al.* (1964) and Rossetti *et al.* (1998). The first assemblage is dominated by imbricated quartz-rich phyllitic and schistose tectonites (Verrucano series) along with minor white marble. In these rocks, a complex metamorphic paragenesis has revealed a polyphased evolution characterized by an early HP/LT phase followed by a LP/HT stage (Rossetti *et al.*, 1998).

Serpentinized ultramafic rocks, as well as metamorphosed gabbros and basalts (Biancone and Tucci, 1984) make up a second imbricated assemblage that occurs as thrust slices within the rocks described above; this tectonic melange shows evidence of a metamorphic evolution similar to that detected in the first assemblage. The third assemblage consists of well-bedded grey limestones, dolostones and solution breccias («Cavernoso») which generally lack a tectonic fabric although observed subhorizontal deformation fabrics include cataclastic slip surfaces parallel to bedding or to the axial planes of recumbent folds. Rocks in the Mesozoic assemblages trend N-S with dips for their respective fabrics being predominantly gentle and toward the west. Observed contacts between these lithologically and tectonically different assemblages are either shallow-dipping shear surfaces or steeply-dipping normal faults.

The entire package of Mesozoic rocks is separated from the GMI by a sinuous, steeply-dipping normal fault, referred to here as the Western Border Fault (WBF). Monzogranite along the east side of the WBF is mylonitized with a gneissic fabric, while sedimentary rocks on the west side show no evidence of *in situ* thermal influence from the GMI. This absence of such metamorphism indicates that the amount of movement on the fault has exceeded the thickness of the original contact aureole surrounding the pluton. Intrusive contacts of the GMI with the surrounding country rock are preserved only at the northern tip of the island where the contact dips gently toward the north, truncating the even more-gently dipping foliation of the hornfelsed argillaceous metasediments.

3. Petrographic outlines

The main Giglio intrusion, the GMI, displays a monzogranite composition throughout. Two mappable facies have been recognized

within this pluton, namely the Arenella Facies (ARF) and Pietrabona Facies (PBF) as shown in fig. 1 (Westerman *et al.*, 1993). Rocks of ARF contain abundant 2-3 cm long megacrysts of orthoclase (fig. 2a), only rarely showing alignment, set in a medium-grained, homogeneous matrix. This texture is in contrast to that of the PBF rocks (fig. 2b) which are non-porphyric and are distinctly foliated as recognized by: i) the alignment of foliated xenoliths and flattened mafic microgranular enclaves; ii) the preferred orientation of biotite and feldspar crystals as well as quarz ribbons; and iii) a modal banding with concentrations of biotite and cordierite in layers a few centimetres thick that erode preferentially with respect to the alternating quartzofeldspatic horizons foliations in the PBF rocks exhibit a rough parallelism to their contact with ARF rocks, and generally dip toward the west. The contact between the ARF and PBF is somewhat gradational, particularly in the northern portion of the island where the transition between facies occurs over a thickness of approximately 200 m. Additionally, PFB rocks are slightly finer grained and darker than ARF rocks; elevated color index values reflect percentages of biotite (20% in PBF *versus* 15% in ARF).

All the GMI rocks consist of the same primary mineral assemblage, namely dominant K-feldspar, plagioclase, quartz and biotite with minor muscovite, tourmaline, apatite and zircon, and the ubiquitous presence of strongly pinitized cordierite. Garnet, andalusite, monazite, titanite and rutile occur sporadically. K-feldspar compositions in the GMI generally have 20-25% Ab in solid solution except in isolated leucocratic masses less than 1000 m^2 in area that occur locally at two north-central locations within the ARF. These leucocratic rocks consist of the same minerals as ARF rocks, but they have higher quartz and lower biotite contents as well as more sodic alkali feldspar (Ab_{33-35}).

Subhedral plagioclase a few millimetres in diameter are a dominant framework phase in all the GMI rocks, displaying strong oscillatory zoning with average compositions near An_{40}. Biotite crystals in ARF and PBF rocks also display zoning, in this case weak, with iron-enriched rims (iron/magnesium ratio grading from 0.52 to 0.57). Microscopic textural characteristics of the PBF rocks include: i) biotite crystals that are smaller than in ARF rocks and show deformation features such as kinks or, more rarely, shreading, ii) mozaic quartz in highly elongated ribbons less than 1 mm thick, and iii) preferred c-axis alignment of plagioclase.

The mineralogical similarities of ARF and PBF rocks reflect the overall similarity of their chemical compositions (table I), but PBF rocks are characterized by higher contents of MgO, Al_2O_3, and to a lesser extent FeO*, and lower CaO (Westerman *et al.*, 1993). The range of SiO_2 is decidedly limited (66.6-68.3%), but the two facies do, in fact, exhibit differences: PBF rocks average 67.3% while ARF rocks average 67.8%. These and other petrographic and geochemical characteristics led Westerman *et al.* (1993) to conclude that the chemical differences between the PBF and ARF are the result of limited fractional crystallization processes with associated decrease in biotite and increase in K-feldspar and quartz.

Based on geological, petrological, geochemical and isotopical evidence, Westerman *et al.* (1993) interpreted the GMI to be a single intrusive body structurally and compositionally zoned. The non-porphyritic and foliated more mafic PBF makes up the western part of the external shell of the intrusion while the porphyritic ARF rocks constitute the core. It is also in this core that leucofacies of the GMI are found, and the younger leucocratic Scole monzogranite intrusion was emplaced along the eastern shoreline. Based on the fabric of the PBF rocks near the contact and on the morphology of the island, the ARF-PBF contact is interpreted to dip moderately toward the west along most of its length.

4. The geomagnetic survey

To verify the geological interpretation of the ARF-PBF contact, we propose a modellistic interpretation of geomagnetic signals joined to the two plutonic facies. To all appearances, the review of petrological and geochemical characteristics of ARF and PBF does not justify a different geomagnetic activity in the two

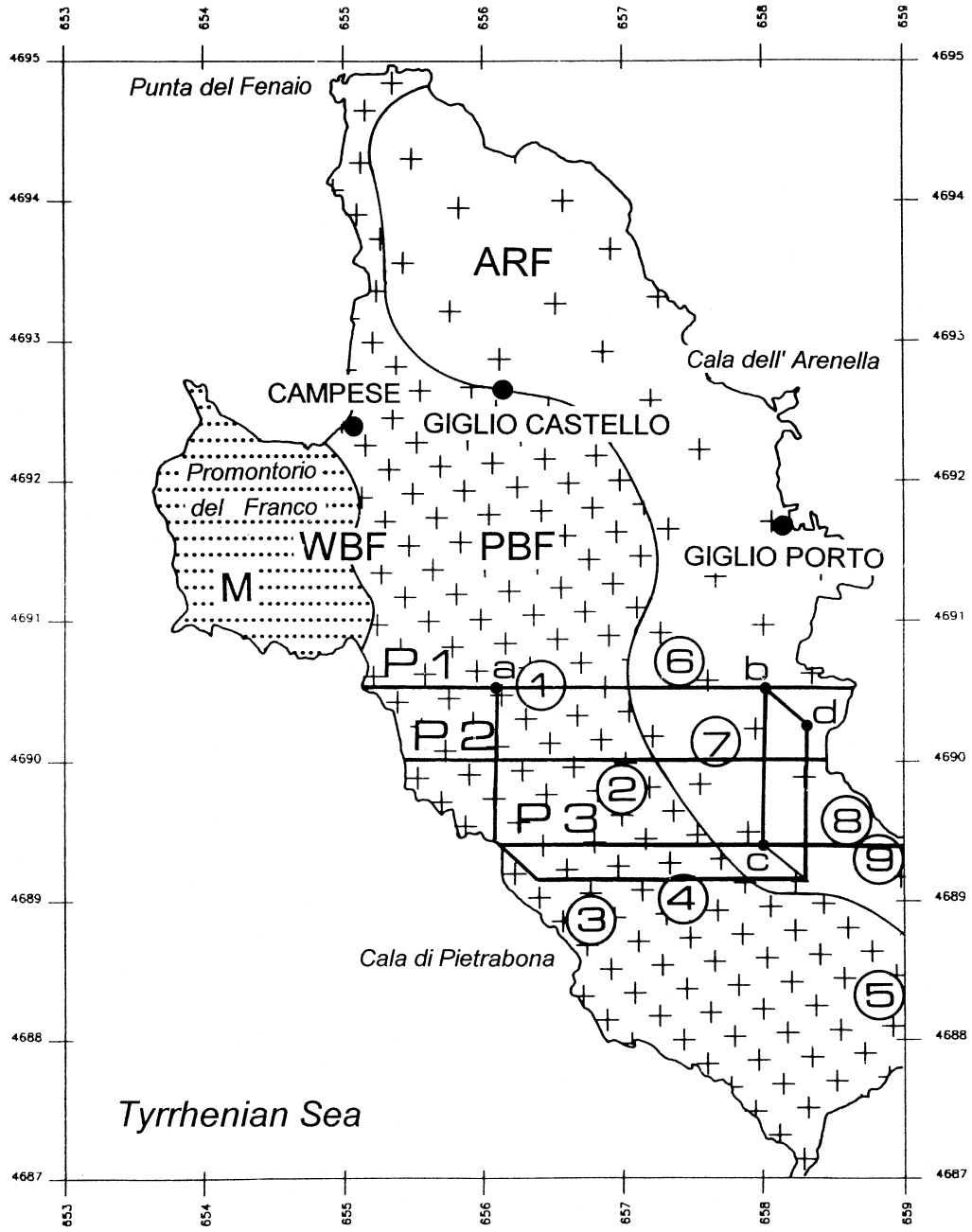

Fig. 1. Map of the Island of Giglio showing the Arenella facies (ARF) – Pietrabona facies (PBF) contact and the Western Border Fault (WBF). P1, P2 and P3 are the traces of two-dimensional modelling profiles; the box (corners a, b, c, d) indicates the volume of the 2D½ model; circled numbers are the locations of the magnetic susceptibility (χ) sampling sites (N hemisphere).

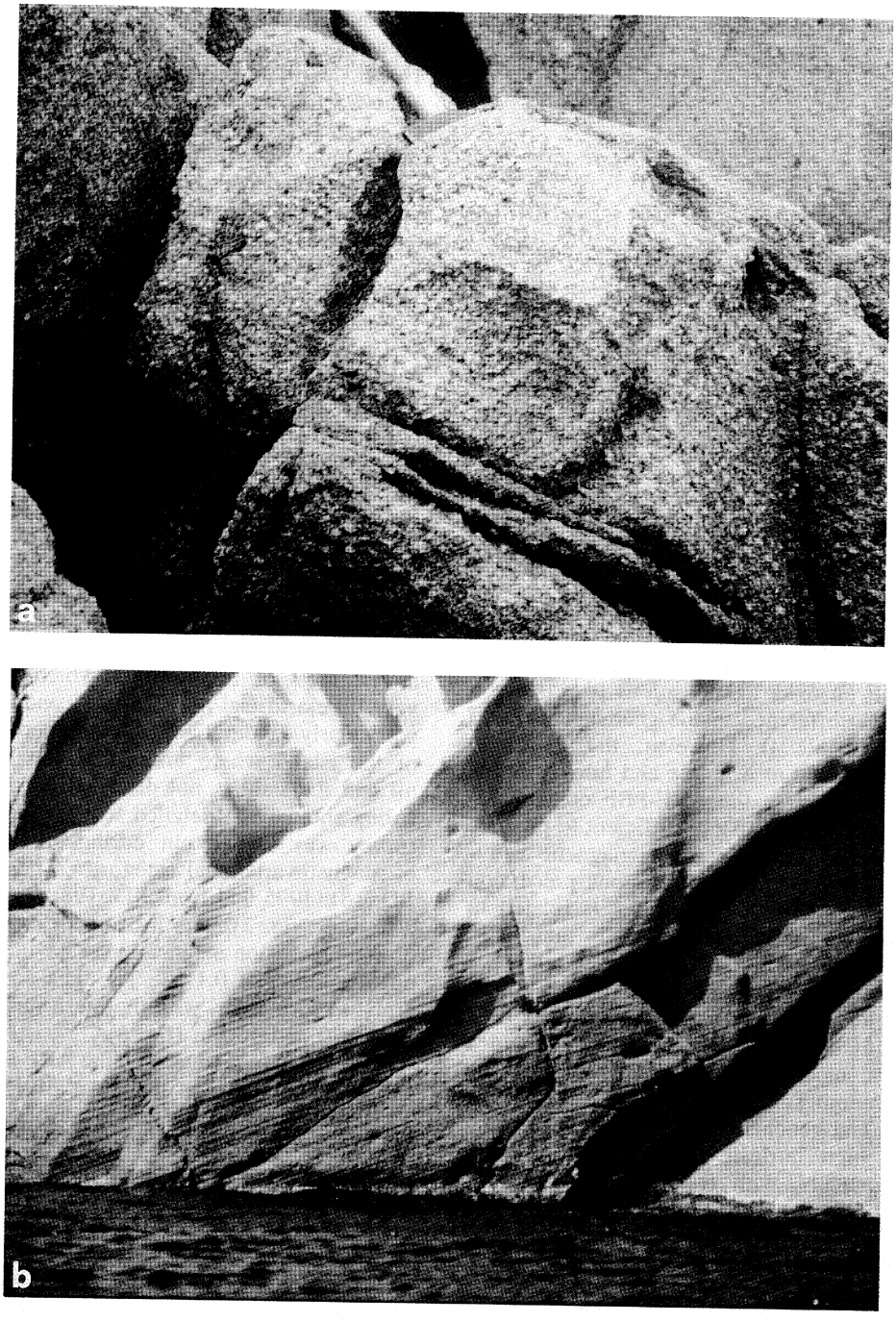

Fig. 2a,b. a) Arenella facies texture illustrating the diagnostic presence of 2-3 cm long orthoclase megacrysts; b) Pietrabona facies texture illustrating the igneous layering that characterizes that facies.

Table I. Average composition of GMI and SMI rocks.

	ARF	PBF	Scole
No. samples	6	6	2
SiO_2	67.83	67.31	70.24
TiO_2	0.67	0.64	0.47
Al_2O_3	15.38	15.80	15.64
Fe_2O_3	1.12	1.13	1.16
FeO	2.65	2.67	1.43
MnO	0.06	0.06	0.04
MgO	1.20	1.34	0.79
CaO	2.10	2.01	1.54
Na_2O	2.79	2.87	2.59
K_2O	4.91	4.81	4.80
P_2O_5	0.24	0.23	0.17
LOI	1.07	1.14	1.17

bodies. One would not expect the similar ARF and PBF Fe oxide compositions to produce a detectable difference in the geomagnetic field intensity (table I). However, the χ survey shows a clearly measurable and homogeneous contrast related to the ARF-PBF contact (table II) (fig. 1). This $\Delta\chi$ is sufficient to produce an intensity difference of geomagnetic activity evaluable by magnetic protons precession methodology. The origin of $\Delta\chi$ is related to structural characteristics of ARF and PBF; probably the PBF rock foliation produces a homogeneous orientation of magnetic mineralogic elements. We use the geomagnetic field related to the ARF-PBF contrast to obtain a structural model of the contact to verify the model coming from the geological, petrographic and geochemical evidence.

The high intrinsic sensitivity of modern magnetometers, with resolution powers well below 1 nT, theoretically allows determination of the nature of contacts between units with low susceptibility contrast. Such a case has been verified on the Island of Giglio where the two igneous facies (ARF and PBF) exhibit a low susceptibility difference. The time variations of the Earth's magnetic field are of fundamental importance in geomagnetic surveys in areas characterized by small anomalies. These variations at intermediate latitudes can achieve values greater than 50 nT, even in quiet geomagnetic conditions, which are significantly more intense than the geomagnetic signals associated with horizons of low susceptibility contrast, and, therefore, careful temporal reduction is necessary (Campbell, 1989; Meloni and Molina, 1989; Schlapp and Butcher, 1995; De Sanctis, 1993; Meloni, 1993).

The geomagnetic environment of the Island of Giglio presents two different contrast horizons. The first one, very strong, is associated with the contact between the GMI, that constitutes the vast majority of the island, and the Promontorio del Franco to the west. The second one, less pronounced, corresponds to the contact between the ARF and PBF (fig. 1). The geomagnetic signal associated with the first contact line is clearly evident in a high definition geomagnetic survey, but the second one, in spite of its low value, can also be resolved since the island is characterized by a low level of urbanization which produces very little artificial noise. These conditions are particularly favourable in the southern portion of the island where urbanization is virtually nil and the field is not distorted by the other strong anomaly. A detailed scalar geomagnetic survey was carried out during six days, all of magnetovariational category *Q*, namely the J.D. 181:1995 and from J.D. 198:1995 to J.D. 202:1995 (fig. 3). The instrument used was a proton precession magnetometer having a readout resolution of 0.1 nT. The data acquisition array was irregular, with the mesh ranging between 20 and 150 m (fig. 6).

The anomaly produced by the ARF-PBF contact is quite weak, on the order of 15-20 nT. Thus, two important conditions must be satisfied in order to obtain a significant model:

a) The time variation of the geomagnetic field must be carefully monitored, in order to maintain accuracy in the time reduction.

b) The magnetic susceptibility of the exposed lithologies must be locally measured in order to have the correct evaluation of the contrast horizon along the ARF-PBF contact line (Bozzo *et al.*, 1984).

Table II. Magnetic susceptibility characteristics of GMI.

Station	No. samples	Facies	χ (emu · 10^{-3})	$\Delta\chi$ (emu · 10^{-3})
1	23	PBF	0.20	0.02
2	24	PBF	0.21	0.01
3	27	PBF	0.22	0.01
4	22	PBF	0.21	0.01
5	23	PBF	0.19	0
6	13	ARF	0.05	0
7	10	ARF	0.08	0.01
8	12	ARF	0.06	0
9	25	ARF	0.04	0

χPBF average = 0.21 · 10^{-3} emu; χARF average = 0.06 · 10^{-3} emu; $\Delta\chi$ (PBF-ARF) = 0.15 · 10^{-3} emu.

Strict control of the Q level temporal variations was obtained by installing an observatory in Passo della Cappelletta, East Liguria (Lat. 44°29′49″.1 N; Long. 09°39′49″.1 E), where a second proton precession magnetometer, having the same characteristics as the field instrument, recorded the magnetogram of the earth field during the period of the survey. The two magnetometers were previously tested at the observatory in Passo della Cappelletta by comparing their measurements for a period of 10 h. Analysis of the two magnetograms demonstrated an r.m.s. deviation of 0.2 nT, with the maximum deviations in the range of ± 1 nT. Temporal sequences recorded in the observatory during the survey (fig. 3) were used as reference for the temporal reduction. The deconvolution was performed by using the technique of the time-lines.

In effect, in the area of the Island of Giglio, when the geomagnetic condition cannot be classified as slow perturbation (K = 0-1 the usual time geomagnetic variations of class *Sq* in a Q day), the time variations have amplitudes of the same order or even larger than the geomagnetic space variations. Moreover, these time variations are different from the corresponding changes observed at the Passo della Cappelletta geomagnetic observatory. These differences cannot be neglected in the high definition geomagnetic survey, and then our geomagnetic observatory is effective for the Giglio area time reduction only in Q day conditions. These conditions were verified in our survey time (fig. 3). (Menvielle and Berthelier, 1991; Menvielle *et al.*, 1995; Chandrasekhar and Alex, 1996; Faggioni *et al.*, 1996).

The resulting map of the observed total intensity geomagnetic field, temporally reduced to J.D. 199:1995 at 06:00 was then submitted to the polar reduction (Tarlowski *et al.*, 1996). The polar reduction procedure, always a distortion of geomagnetic field natural structure, is very useful to obtain the geometry of the anomaly field. The analytic expression of small anomalous geomagnetic sources in high definition prospecting is written as a convolution of three space functions: the first one f_a, named also «amplitude factor», depends on magnetic moment per unit volume; the second one f_h, «depth factor», depends on the anomalous body pole depth; the third one f_β, «field-orientation factor» is $f_\beta = (l\cos\beta + m\,\mathrm{sen}\,\beta)^2 + n^2$ where β is the angle between the dipole axis of the anomalous source and magnetic N and l, m, n are F direction cosines. In the present case, the lateral extent of the geomagnetic source is large compared to its depth («large scale sources») and two additional factors are necessary in order to describe such magnetic fields

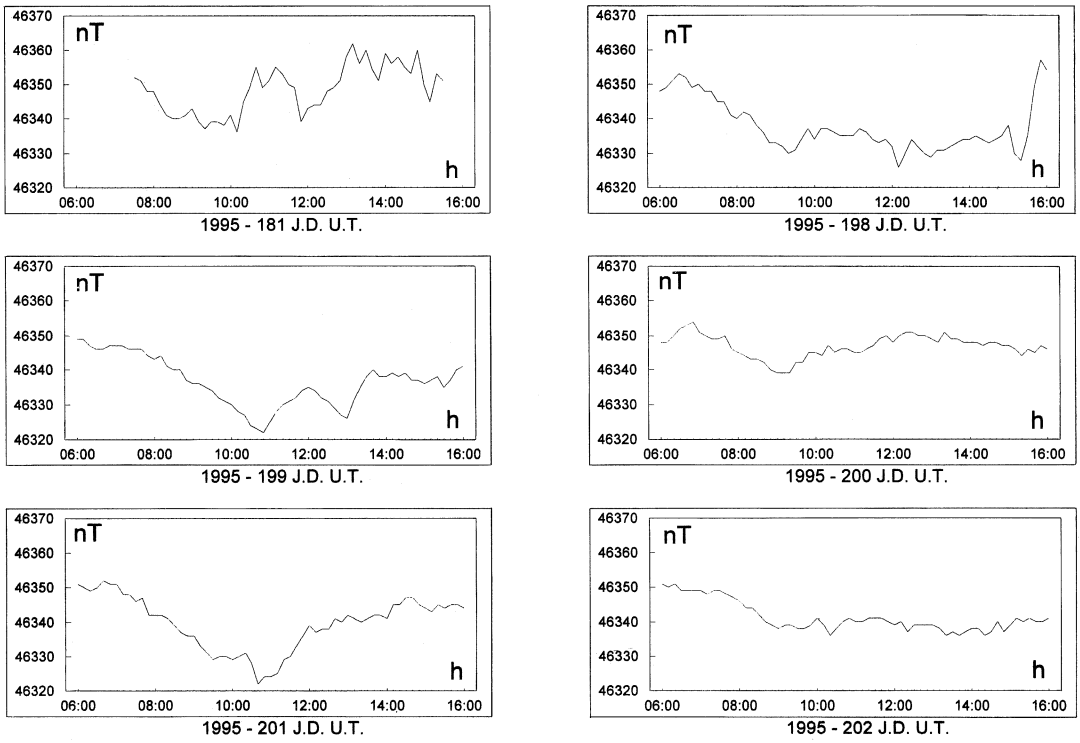

Fig. 3. Magnetograms of the total intensity geomagnetic field F, recorded in Passo della Cappelletta geomagnetic station.

efficaciously: f_s, «size factor», and f_o, «polarization-orientation factor», related to direction cosines of the polarization vector. The factors f_β and f_o have directional effect in the anomaly field, and in the present case where geometric information of the orientation of the source (ARF-PBF contact) is needed, these effects must be erased. This operation is the reduction to the pole, that computes the change from the local inclination of the geomagnetic field to the vertical direction by convolving the observed geomagnetic field with a filter whose frequency response is the product of f_β and f_o functions (Gunn, 1975; Telford *et al.*, 1990).

The polar reduced map (fig. 4b), obtained using $i = 58°00'00''$ and $d = 0°05'$ (+) computation parameters, shows that the strong spatial field variation is connected to the ophiolite-rich assemblage of Promontorio del Franco and to iron oxide mineralization along the WBF plane; the amplitude of the variation can be qualitatively estimated at about 85 nT with a spatial extension of 700 m approximately in the direction orthogonal to the fault (fig. 4a,b).

Also evident in fig. 4a,b is an alignment of maxima and minima that seems to parallel the ARF-PBF contact, particularly in the southern part of the island where distortion due to the strong WBF anomaly is reduced. This effect becomes clearer by developing the residual of the measured field. The most detailed regional reference field available in the area is the ItGRF, but it is not suitable for the purposes of this study because the Giglio anomalies are generated from very superficial structures and are, therefore, characterized by very short

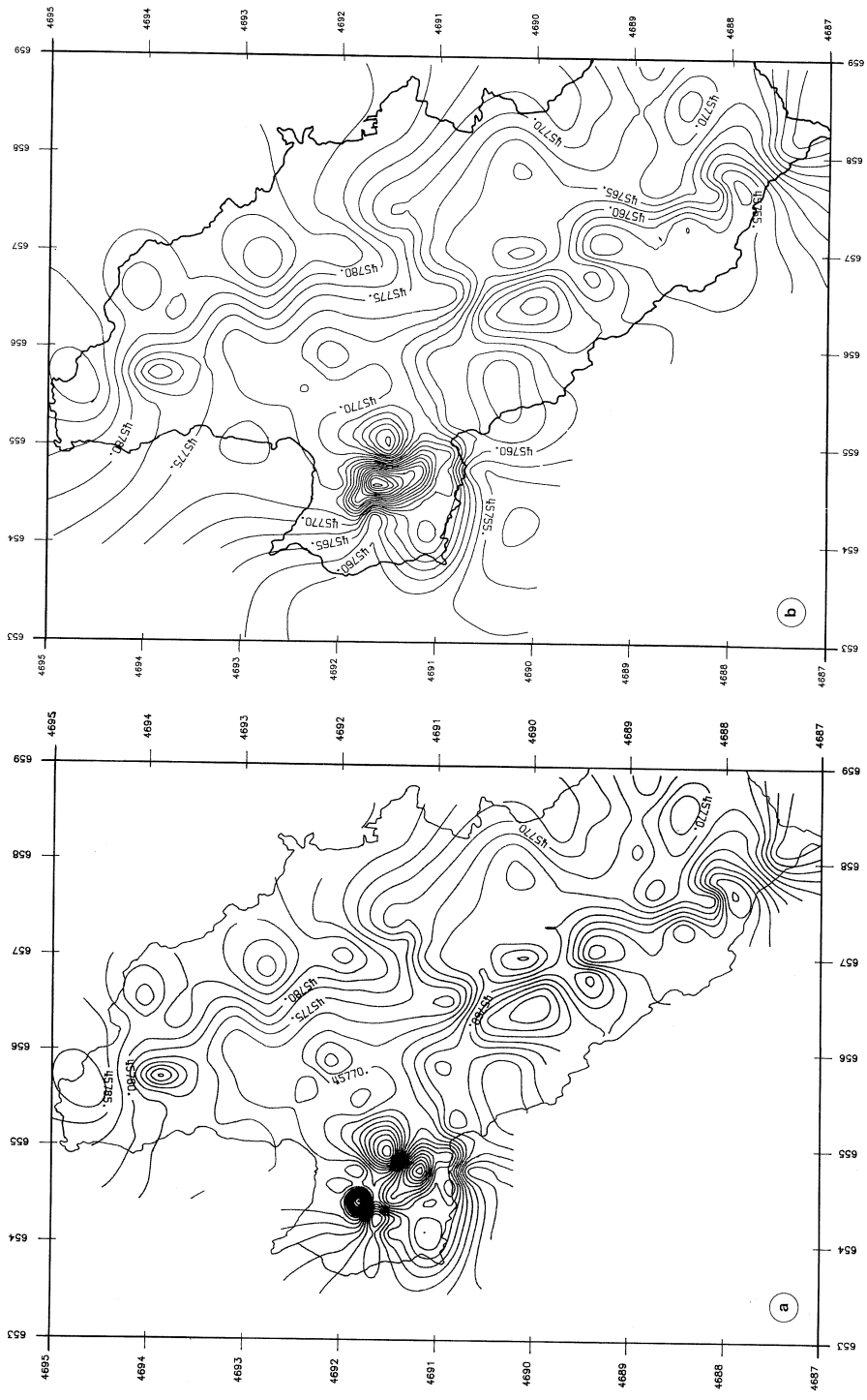

Fig. 4a,b. a) Map of total intensity geomagnetic field F of the Island of Giglio. Isomagnetic line every 2.5 nT. Coordinates in UTM km (N hemisphere). b) Map of pole-reduced total intensity geomagnetic field F of the Island of Giglio. Isomagnetic line every 2.5 nT. Coordinates in UTM km (N hemisphere). Polar reduction parameters: $i = 58°00'00''$; $d = 00°05$ (+).

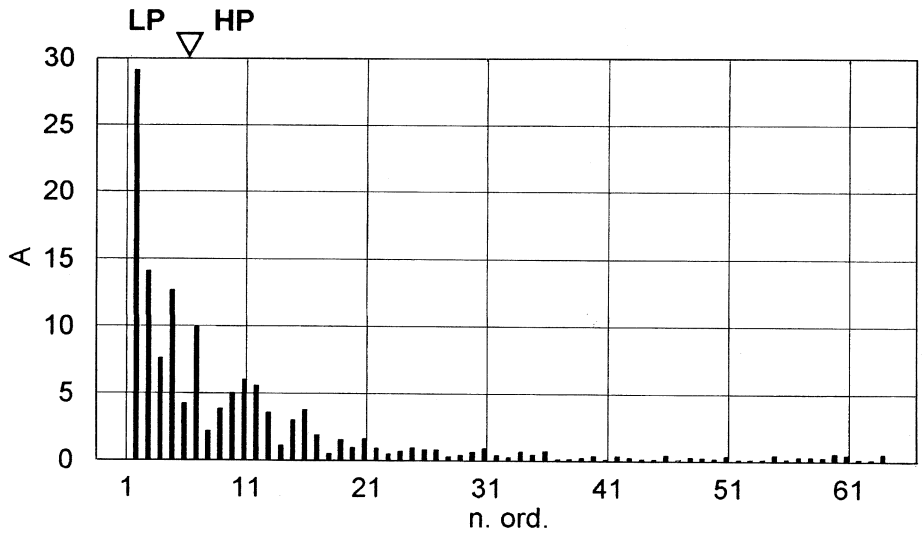

Fig. 5. FFT amplitude spectrum of the measured field (λ_{max} = 4.5 km; λ_{min} = 0.15 km). Amplitude on the abscissa; wave numbers on the ordinate.

wavelengths (λ < 1 km). Accordingly, a spectral FFT process was used to develop the residual (Lowes, 1974; Faggioni *et al.*, 1997). Figure 5 presents the amplitude spectrum of the Earth's magnetic field in the wavelength band between 4.5 km and 0.15 km. The cut-off wavelength of 1.1 km, corresponding to the spectral order number 4, was chosen to obtain an *Lp* field characterized only by contributions from the deepest local anomaly geomagnetic sources (Spector and Grant, 1985; Bozzo and Faggioni, 1986, Faggioni *et al.*, 1997). The spectral reference field, obtained by operating a low-pass filtering at 1.1 km, is characterized by an amplitude low of about 40 nT centered on the PBF southeast of the exposed portion of the WBF. The SRF (Spectral Reference Field) (fig. 6) excludes the most coastal stations to control the coastal effect and to erase the border effect. The extension out side of the survey is due to the computed extrapolation and has no physical meaning. In this field, the strongly superficial WBF anomaly is almost completely filtered out (the residual distortion at the fault is less than 5 nT – 6% of the observed anomaly), while the anomalies connected with the PBF-ARF contact have disappeared. The corresponding map showing the spectral anomaly field resulting from high-pass filtering (fig. 7) clearly confirms the alignment of anomalies along the southern PBF-ARF contact as revealed on the ground, and indicates the amplitude of this geomagnetic contrast horizon as 10-15 nT (Hsu *et al.*, 1996).

5. The geomagnetic model

The model used to explicate the anomalies associated with the ARF-PBF contact surface refers to a total rock volume ab · bc · bd, contained between the parallels 4689.3 N (UTM km) and 4690.5 (UTM km) and meridians 656.1 E (UTM km) and 658.0 E (UTM km) with a depth of 0.3 km (fig. 1). This model was constructed by integrating information from three different sources: the geomagnetic signal, the ARF-PBF contact as observed from the geological surface survey, and the difference between the magnetic susceptibilities deduced from experimental measurement on samples of the two facies. The modelled volume was cho-

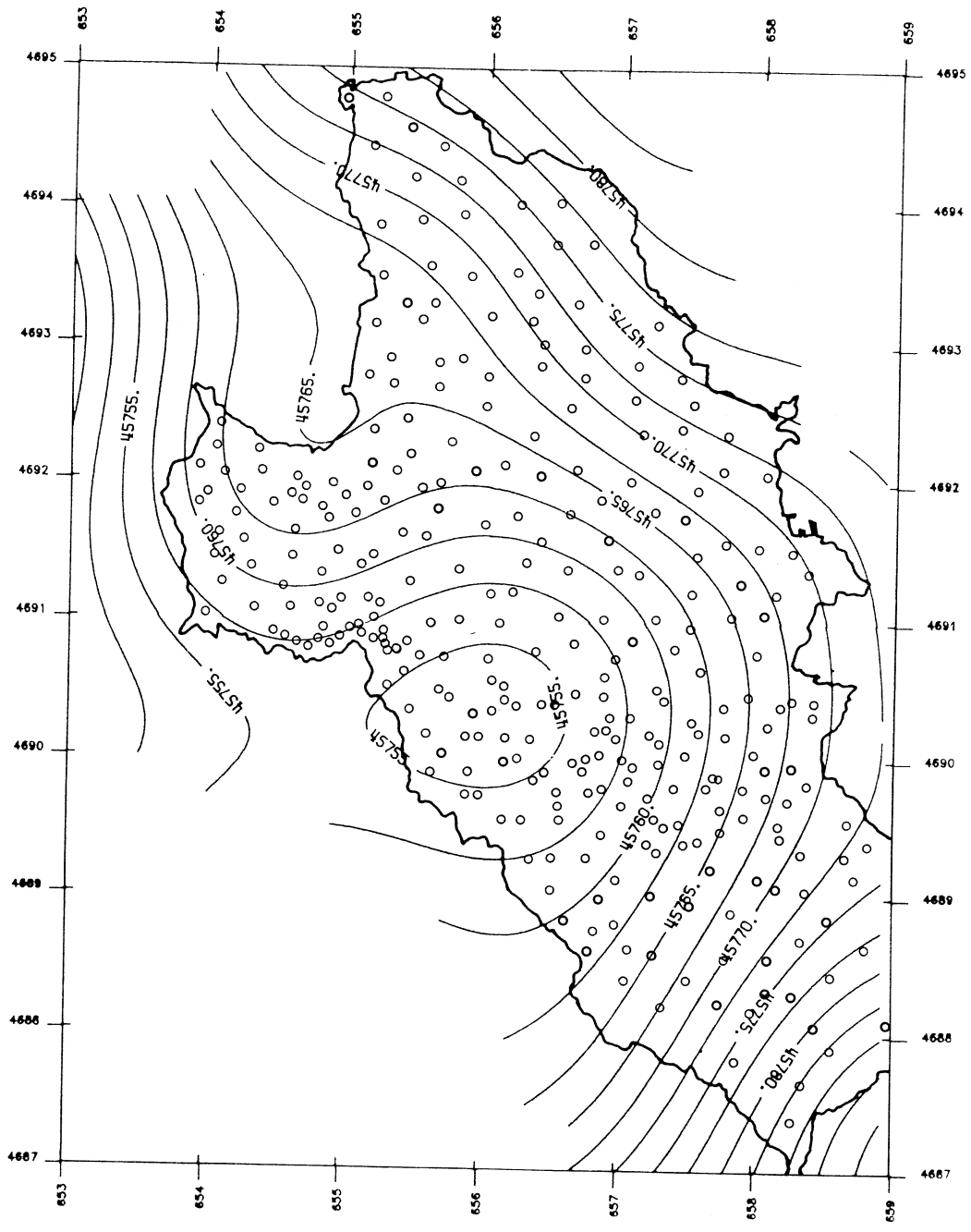

Fig. 6. Spectral reference field of the total intensity geomagnetic field of the Island of Giglio. LP filter cut-off at 1.1 km. Isomagnetic line every 2.5 nT. Coordinates in UTM km (N hemisphere). White circles are measurement stations.

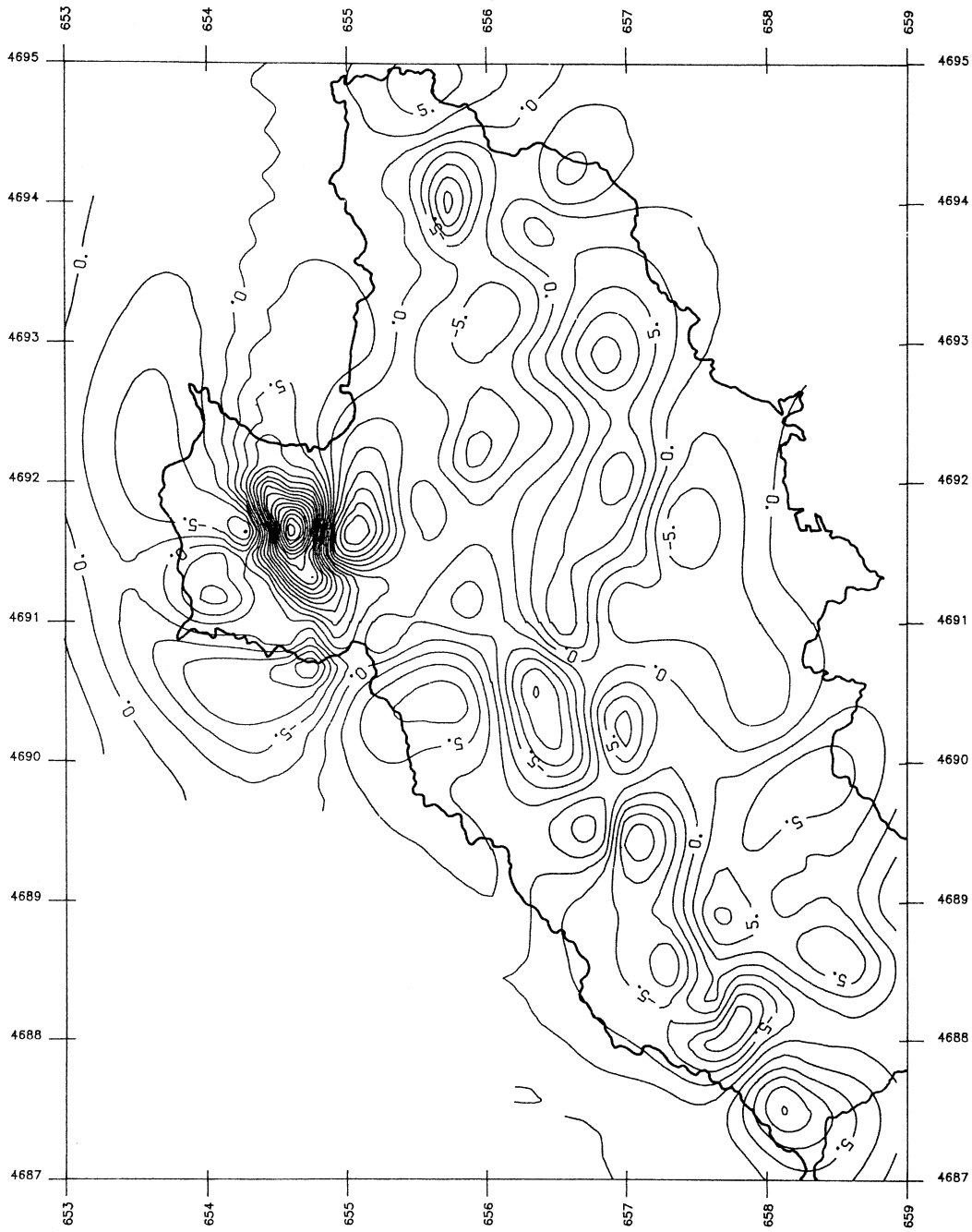

Fig. 7. Spectral anomaly field of the total intensity geomagnetic field *F* of the Island of Giglio. LP filter cut-off at 1.1 km. Isomagnetic line every 2.5 nT. Coordinates in UTM km (N hemisphere).

sen because it has very low urbanization and is sufficiently distant from the WBF structure to avoid its perturbation effects.

The horizontal derivative of the geomagnetic field gives a first constraint to the model. The maximum of the horizontal derivative of the field generated by a crustal source is located on its vertical projection (Faggioni *et al.*, 1997). Thus, if the discontinuity is a vertical plane, the line connecting the derivative maxima should coincide with the geological contact. The scalar derivative field has been calculated in this case from the spectral anomaly map. The resulting horizontal derivative map (fig. 8) shows that the line connecting the maxima (show by a bold line) lies parallel to the ARF-PBF contact as mapped in the field, but it is shifted westward a distance ranging from 0.7 and 1.1 km. This relationship is particularly clear in the southern part of the island, and provides evidence that the geological contact between these facies dips toward the west, in agreement with the existing geologic interpretation (Westerman *et al.*, 1993). This situation is not clear further north were the ARF-PBF contact is near the coastline (100-200 m) and the low geomagnetic effects due to the bodies' structural differences are overmodulated and distorted by the coastal effect. The geomagnetic high corresponding to the PBF north of Promontorio del Franco, is probably located out to sea, but this signal will not be measurable by current marine geomagnetic methodology because it is too low and is overmodulated by the WBF geomagnetic signal.

As stated above, the geomagnetic anomaly associated with the ARF-PBF contact is really quite weak. Thus, it was necessary to make *in situ* measurements of the magnetic susceptibility χ of the two facies in order to obtain a realistic geometric model of the crustal structure by the inversion technique. About 150 susceptibility determinations were made using a portable k-meter at nine different sites, four in the ARF domain and five in the PBF domain (fig. 1); results are summarized in table II. Since measured values are quite homogeneous for each facies, it seems reasonable to assign the average measured values as the typical susceptibilities of the two lithologies. Modelling has been carried out in two steps: first in two dimensions along parallel E-W sections, and second in 2D½ by modellistic integration of the two-dimensional models. The two dimensional sections were calculated on the P1, P2, and P3 magnetic profiles (fig. 1) by assuming magnetic susceptibility contrasts of 0.18, 0.15 and 0.15 emu/10^3, respectively. In fig. 9, values of locally measured magnetic anomalies (crosses) and values calculated from the model (circles) are superimposed on plotted topographic profiles. Below each profile, a geomagnetic model is plotted with the line fitting the corners of this computed model. The resulting values of the inclination angle of these computed lines are $\alpha_1 = 54°$, $\alpha_2 = 21°$ and $\alpha_3 = 44°$, respectively. On the topographic profile, the ARF-PBF contact is indicated (black circle marker) as constructed from the geological data, along with an error of location of 550 m for P1, 200 m for P2, and 150 m for P3.

The 2D½ model shown in fig. 10 was constructed in two steps from the two-dimensional models. The first step gave the longitudinal and depth model coordinates of computed profiles 4 and 5, located parallel to the measured profiles and equidistant between them. It was assumed in this interpolation that the weights of the models 1, 2 and 3, were $W_1 = W_2 = 0.92$ and $W_3 = 0.08$ for calculating profile 4, and $W_1 = 0.08$ and $W_2 = W_3 = 0.92$ for calculating profile 5. Calculations of the inclinations for profiles 4 and 5 produced values of $\beta 4 = 37°$ and $\beta 5 = 32°$. Finally, the 2D½ model of the contact separating the two volumes ARF and PBF was generated by geometric interpolation between the longitude and depth of the five two-dimensional model corners.

6. Conclusions

The low difference in magnetic susceptibility between the plutonic facies ARF and PBF is the source of a weakly anomalous geomagnetic signal. This anomaly field is well resolved with standard geomagnetic field instrumentation such as a proton precession magnetometer. Using a coastal geomagnetic reference

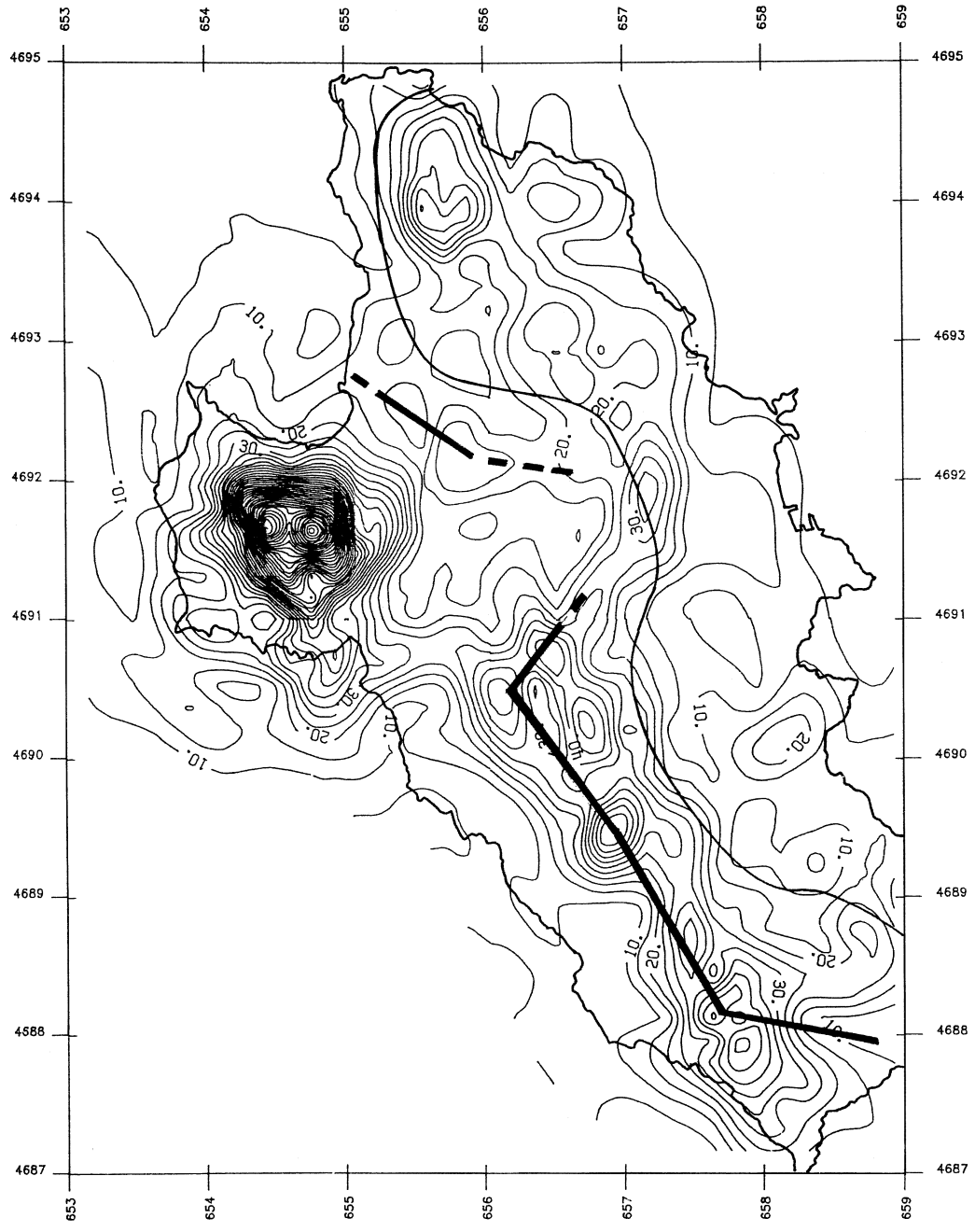

Fig. 8. Horizontal derivative map of the anomalies calculated from fig. 7. Isomagnetic line every 10 nT/km. Thin line shows ARF-PBF geological contact; bold line connects the maxima points of the horizontal derivative (N hemisphere).

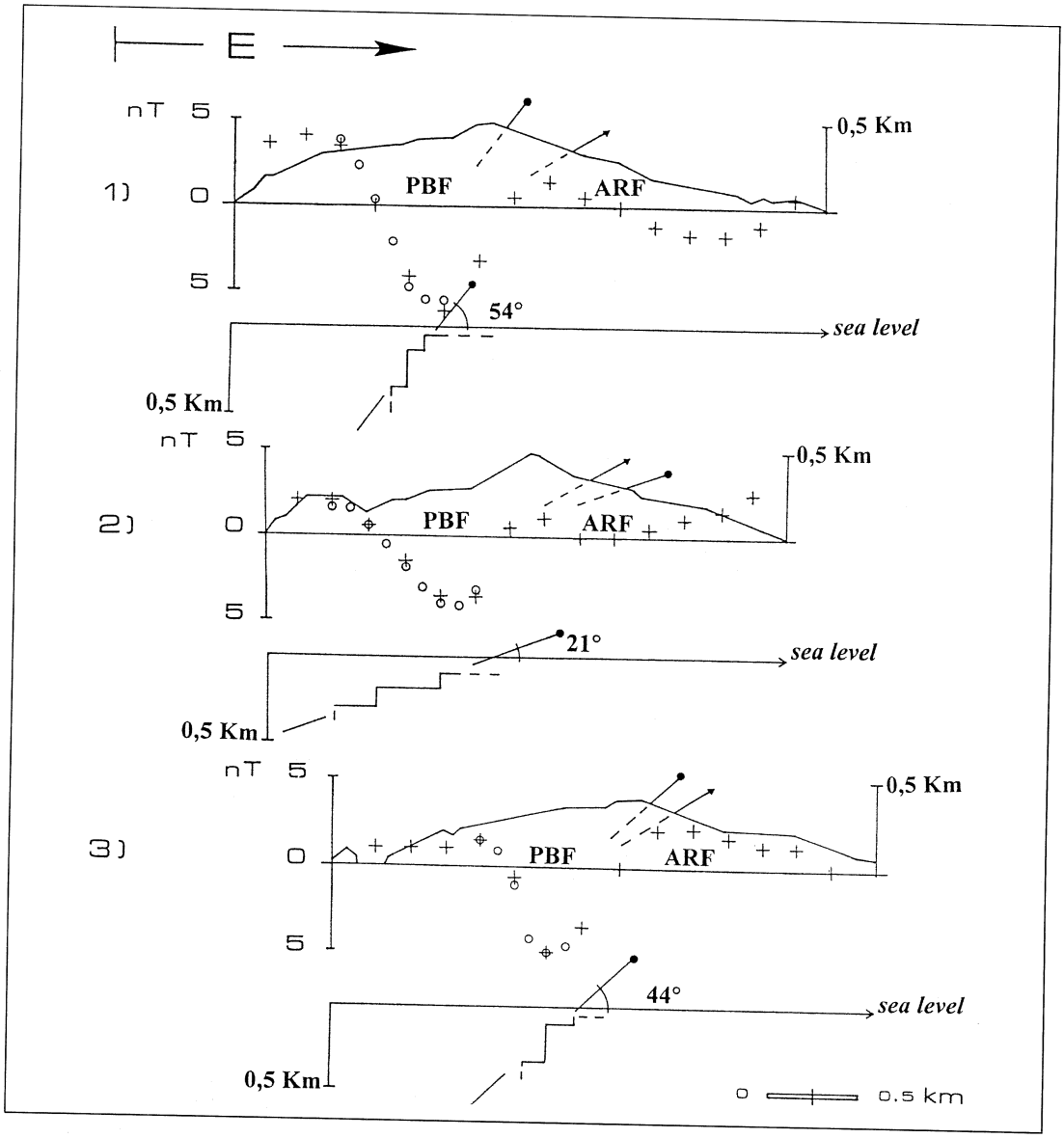

Fig. 9. Two-dimensional models of geomagnetic sections P1 (from 655.23 E to 658.62 E, lat. 4690.52 N UTM km), P2 (from 655.44 E to 658.43 E, lat. 4690.00 N UTM km), P3 (from 655.85 E to 659.00 E, lat. 4689.35 N UTM km). Cross point: geomagnetic field along profiles P1, P2, P3 from graphic matrix. Open circle points: geomagnetic field computed from the geometric structural model. Magnetic susceptibility differences $\Delta\chi = \chi_{PBF}-\chi_{ARF}$: 0.18 (P1), 0.15 (P2), 0.15 (P3) emu/10^3. In the models: geometric profile of deep ARF-PBF discontinuity, linear interpolation of the inclination angle of the computed models (segments with black circle marker). In the topographic profiles: linear interpolation of position and inclination of modelled ARF-PBF contact (black circle marker); position and estimated inclination of ARF-PBF contact by geological survey (black triangle marker).

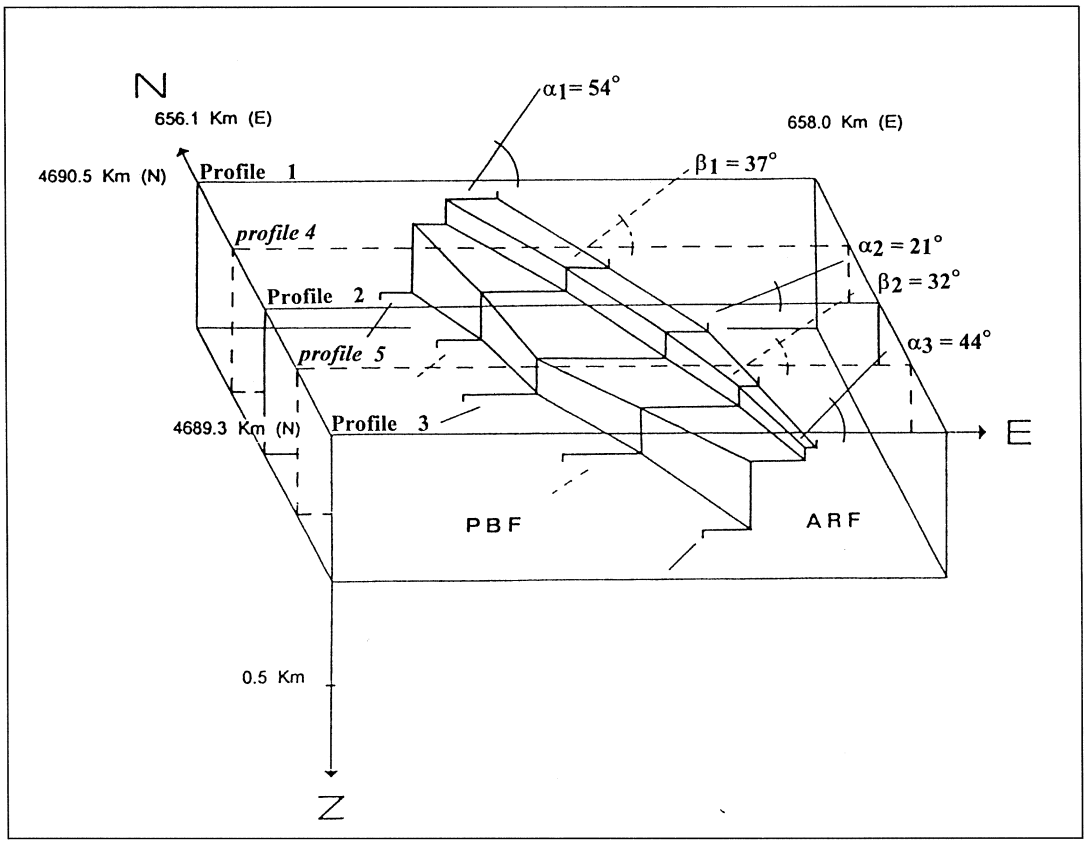

Fig. 10. 2D½ model of the ARF-PBF contact. Models 1, 2, 3 = positions of corners computed from geomagnetic measured profiles; models 4, 5 = positions of corners interpolated from geometric (deep and longitudinal kilometric E distance from meridian 656.1 E Greenwich) position of computed model corners.

observatory, we have verified the *Q* day conditions necessary to make a careful temporal deconvolution, achieving maximum resolution. Low magnetic noise in the local environment and high spatial density of experimentally recorded points make possible the construction of an anomaly field map having a low noise level and presenting detailed magnetic characteristics. Direct correlation between the orientation of the anomalies and the geological contact ARF-PBF results from study of the spectral anomaly field and its horizontal derivative. A 2D½ model obtained from these data demonstrates that the surface separating the ARF and PBF blocks dips to the W, in agreement with the geological evidence observed in the field.

Although the limited extension of the island does not allow a complete 2D½ reconstruction of the intrusion, the gently westward-dipping sinuous trend of the contact between the outer foliated facies and the inner homogeneous one suggests that at least the upper part of the pluton was affected by radial expansion, quite possibly linked to ballooning. More detailed geometrical constraints may be possible as a result of a recently completed, offshore, high-definition magnetic survey.

REFERENCES

BARTOLE, R. (1995): The North-Tyrrhenian-Northern Apennines post-collisional system: constrain for a geodynamic model, *Terranova*, **7**, 7-30.

BIANCONE, M. and P. TUCCI (1984): The ophiolite rocks of Giglio Island (Tuscan Archipelago), *Ofioliti*, **9**, 321-336.

BOUILLIN, J.-P., J.-L. BOUCHEZ, P. LESPINASSE and A. PÊCHER (1993): Granite emplacement in an extensional setting: an AMS study of the magnetic structure of Monte Capanne (Elba, Italy), *Earth Planet. Sci. Lett.*, **118**, 263-279.

BOZZO, E. and O. FAGGIONI (1986): Indagini geostrutturali lungo la linea Levanto-Ottone, *Mem. Descr. Carta Geol. D'Italia*, **35**, 27-32.

BOZZO, E., G. CORRADO, A. ELENA, O. FAGGIONI and E. PINNA (1984): Magnetic anomalies and deep crustal structure along the Elba-Levanto-Ottone-Varzi Line, *Boll. Geofis. Teor. Appl.*, **26** (101-102), 67-75.

BURELLI, F. and P. PAPINI (1991): Structural analysis of Giglio Island pluton (Northern Tyrrhenian Sea), *Geologia del Basamento Italiano*, 109-111.

CAMPBELL, W.H. (1989): The regular geomagnetic field variation during quiet solar variations, *Geomagnetism*, edited by J.A. JACOBS, vol. 3, 385-460.

CHANDRASEKHAR, E. and S. ALEX (1996): On the anomalous features of the geomagnetic quiet-day field variations at Nagpur, India, *Geophys. J. Int.*, **127** (3), 703-708.

DE SANTIS, A. (1993): Tempeste, sottotempeste e baie magnetiche, *Ann. Geofis.*, **36** (suppl. n. 5-6), 55-77.

FAGGIONI, O., E. PINNA, C. SAVELLI and A. SCHREIDER (1995): Geomagnetism and age study of Tyrrhenian Seamounts, *Geophys. J. Int.*, **123**, 915-930.

FAGGIONI, O., N. BEVERINI, C. CARMISCIANO and L. ROSSI (1996): Sulla misura delle variazioni temporali del campo geomagnetico in Provincia della Spezia, 1996, Mem. Accad. Sci. MFN «G. Cappellini», **64-65**, 161-184.

FAGGIONI, O., N. BEVERINI and C. CARMISCIANO (1997): Geomagnetic time variations and high definition study of space magnetic effects induced by artificial submerged source, *Boll. Geofis. Teor. Appl.*, **38** (3/4), 211-228.

GUNN, P.J. (1975): Linear transformations of gravity and magnetic fields, *Geophys. Prospect.*, **23**, 320-312.

HSU, S.K., J.C. SIBUET and C.T. SHYU (1996): High-resolution detection of geologic boundaries from potential-field anomalies: an enhanced analytic signal technique, *Geophysics.*, **61** (2), 373-386.

INNOCENTI, F., G. SERRI, G. FERRARA, P. MANETTI and S. TONARINI (1992): Genesis and classification of the rocks of the Tuscan magmatic province: thirty years after Marinelli's model, *Acta Vulcanol.*, **2**, 247-265.

INNOCENTI, F., D.S. WESTERMAN, S. ROCCHI and S. TONARINI (1997): The Montecristo Monzogranite (Northern Tyrrhenian Sea Italy): a collisional pluton in an extensional setting, *Geol. J.*, **32**, 131-151.

LAZZAROTTO, A., R. MAZZANTI and F. MAZZONCINI (1964): Geologia del Promontorio Argentario (Grosseto) e del Promontorio del Franco (Isola del Giglio), *Boll. Soc. Geol. It.*, **83**, 1-124.

LOWES, F.J. (1974): Spatial power spectrum of the main geomagnetic field and extrapolation to the core, *Geophys. J. R. Astron. Soc.*, **36**, 717-730.

MARINELLI, G. (1961): Genesi e classificazione delle vulcaniti recenti Toscane, *Atti Soc. Tosc. Sci. Nat.*, **68**, 74-116.

MELONI, A. (1993): La variazione secolare del campo geomagnetico, *Ann. Geofis.*, **36** (suppl. 5-6), 41-54.

MELONI, A. and E. MOLINA (1989): Study of the *S* variation at L'Aquila geomagnetic observatory, *Ann. Geophysicae*, **7**, 387-394.

MENVIELLE, M. and A. BERTHELIER (1991): The K-derived planetary indices: description and availability, *Rev. Geophys.*, **29**, 415-532.

MENVIELLE, M., N. PAPITASHVILI, L. HAKKINEN and C. SUCKSDROFF (1995): Computer production K indices: review and comparison of methods, *Geophys. J. Int.*, **123** (3), 866-886.

PASSERINI, P. and M. MARCUCCI (1992): Mesoscopic faults in the granite of Isola del Giglio (Tuscan Arcipelago), *Tectonophysics*, **206**, 265-283.

POLI, G. (1992): Geochemistry of Tuscan Archipelago granitoids, Central Italy: the role of hybridization processes in their genesis, *J. Geol.*, **100**, 41-56.

ROSSETTI, F., C. FACCENNA, L. JOLIVET and R. FUNICIELLO (1998): Structural evolution of the Giglio Island, *Mem. Soc. Geol. It.*, **52**, 493-512.

SERRI, G., F. INNOCENTI and P. MANETTI (1993): Geochemical and petrological evidence of subduction of delaminated Adriatic continental lithosphere in the genesis of the Neogene-Quaternary magmatism of Central Italy, *Tectonophysics*, **223**, 117-147.

SCHLAPP, D.M. and E.C. BUTCHER (1995): Seasonal and sunspot-cycle changes in the day-to-day variability of *Sq*, *Geophys. J.*, **120** (1), 173-185.

SPECTOR, A. and F.S. GRANT (1985): Statistical models for interpreting aeromagnetic data, *Geophysics*, **50**, 1951-1960.

TARLOWSKI, C., A.J. MCEWIN, C.V. REEVES and C.E. BARTON (1996): Dewarping the composite aeromagnetic anomaly map of Australia using control traverses and base stations, *Geophysics*, **61** (3), 696-705.

TELFORD, W.M., L.P. GELDART and R.E. SHERIFF (1990): *Applied Geophysics*, second edition (Cambridge University Press), 108-109.

WESTERMAN, D.S., F. INNOCENTI, S. TONARINI and G. FERRARA (1993): The Pliocene intrusions of the Island of Giglio (Tuscany), *Mem. Soc. Geol. It.*, **49**, 345-363.